Electron energy loss spectroscopy studies of the amorphous to crystalline transition in FeF_3

M. S. M. Saifullah,[a] G. A. Botton,[b] C. B. Boothroyd, and C. J. Humphreys
Department of Materials Science and Metallurgy, University of Cambridge, Cambridge CB2 3QZ, United Kingdom

(Received 3 December 1998; accepted for publication 25 May 1999)

Electron beam-induced crystallization studies in amorphous FeF_3 films using electron energy loss spectroscopy (EELS) are discussed in this letter. Time-resolved EELS studies show that the coordination polyhedra in amorphous FeF_3 (a-FeF_3) are randomly arranged FeF_6 octahedra. They arrange themselves to give long range order during crystallization to FeF_2 and FeF_3 under the electron beam. Changes in the d-band occupancy by one electron as well as the sensitivity of the ratio of the Fe L_3 and L_2 edges to the electronic configuration of the iron ion are clearly seen during the crystallization process. © *1999 American Institute of Physics.* [S0021-8979(99)03817-7]

I. INTRODUCTION

Metal fluorides are attracting a lot of interest in high-resolution electron beam nanolithography because of their self-developing properties.[1–4] Direct electron beam writing on these resists is currently the most promising method for defining ultrasmall nanostructures. Hence, it is important to study their damage characteristics under the electron beam to understand their behavior as inorganic resists. It has been shown that a-AlF_3 (Refs. 5,6) and a-FeF_3 (Refs. 7,8) damage under the electron beam and are sensitive to moisture in the film. Earlier work on a-FeF_3 is confined to Mössbauer spectroscopy,[9] extended x-ray absorption fine-structure spectroscopy (EXAFS) and x-ray absorption near edge structure (XANES)[10] to study the Fe ions in an amorphous environment.

Electron energy loss spectroscopy (EELS) provides valuable information on chemical composition as well as invaluable data on the chemical environment of the excited atoms. The $L_{3,2}$ edges of $3d$ transition metals observed in EELS are marked by ''white lines,'' resulting from the excitation of electrons from the $2p_{3/2}$ and $2p_{1/2}$ spin-orbit split levels to the unoccupied $3d$ states. However, these $L_{3,2}$ edges can split due to the loss of degeneracy induced by the crystal-field potential around the central cation. In crystals with cubic symmetry, this potential splits the d orbitals into two states belonging to e_g and t_{2g} representations. Transitions to these states are therefore observed in the $L_{3,2}$ edges if these states are empty. It is well established that the normalized intensities of transition metal L edges can be correlated with d-band occupancy. It is also shown that amorphous to crystalline transition can be monitored by studying the $3d$ state occupancy in transition metals.[11] In a site specific valence determination study using EELS, the occupation of Fe^{2+} and Fe^{3+} ions in the tetrahedral sites and octahedral sites, respectively, was determined in a mixed spinel.[12] In the present work, the local environment in a-FeF_3 film, the amorphous to crystalline transition and the d-band occupancy are studied using EELS.

II. EXPERIMENT

Commercial iron (III) fluoride powder (>97% pure) was preheated to 300 °C for 6 h to dehydrate before thermally evaporating it onto carbon covered copper grids. A 40 nm thick film was deposited at the rate of 0.2 nm/s. Mössbauer spectroscopy studies of Fe in a-FeF_3 films showed it to have an Fe^{3+} valence state.[9] After the evaporation, the specimen was immediately transferred to a vacuum bottle and placed in the microscope within 10 min of its preparation. The amorphous to crystalline transition studies were carried out in a Philips CM30 transmission electron microscope operated at 100 kV equipped with a LaB_6 filament and a Gatan 666 parallel electron energy loss spectrometer. The energy resolution was better than 1 eV at an energy dispersion of 0.12 eV per channel. The spectra were acquired in image mode with an acquisition time of 12.8 s.

A uniformly illuminated area was obtained by overfocusing the condenser lens C2 and the beam current was adjusted every ~10 min using a picoammeter attached to the viewing screen and any decay in beam current was compensated for. The beam current was measured using the drift tube of the spectrometer. Diffraction patterns were recorded by irradiating adjacent areas of specimen for different times.

III. RESULTS AND DISCUSSION

The three diffraction patterns in Figs. 1(a)–1(c) show the crystallization process with the increasing electron dose. It is observed that the deposited film is amorphous and with the increasing electron dose it begins to crystallize. It is seen that at low doses ($\sim 1\times10^6$ C m^{-2}) FeF_2 appears while the extra reflections at higher doses correspond to FeF_3. Figure 1(d) shows the diffraction patterns acquired after a dose of 1.1×10^6 C m^{-2} (top) and 3.3×10^6 C m^{-2} (bottom) to identify

[a]Nanostructure Technology Research Group, Device Physics Research Laboratory, NTT Basic Research Laboratories, 3-1, Morinosato Wakamiya, Atsugi-shi, Kanagawa Pref., 243-0198, Japan; electronic mail: saif@aecl.ntt.co.jp
[b]Also at Materials Technology Laboratory, CANMET, 568 Booth Street, Ottawa, Ontario KIA 041, Canada.

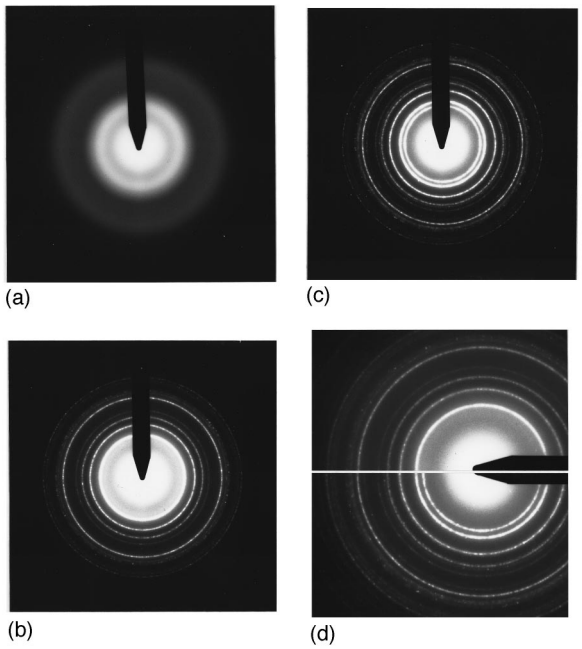

FIG. 1. Selected area diffraction patterns taken with increasing electron dose during the amorphous to crystalline transition in a-FeF_3 (a) as prepared, (b) 1.1×10^6 C m^{-2}, (c) 3.3×10^6 C m^{-2}, and (d) shows the position of the rings of FeF_2 and FeF_3 (see Fig. 2 for details).

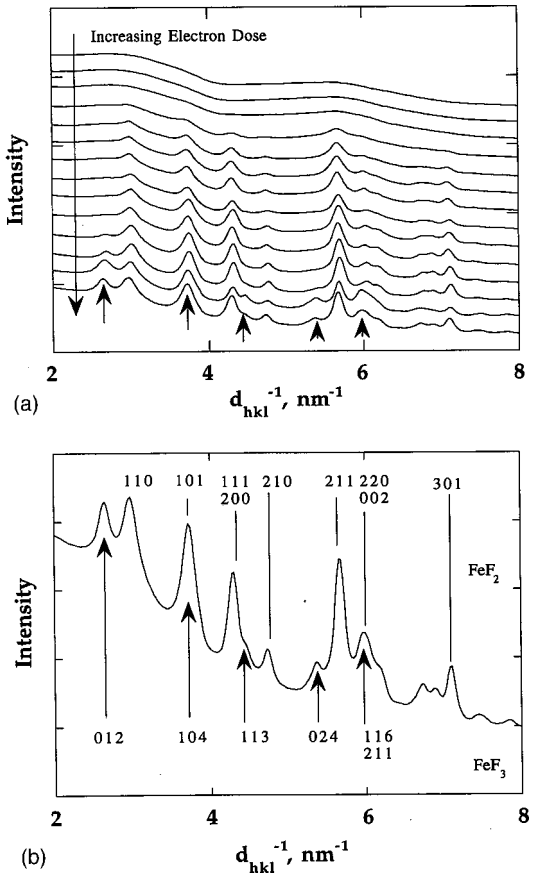

FIG. 2. (a) Radially averaged diffraction patterns of the dry thermal film as a function of electron dose, increasing upto 3.3×10^6 C m^{-2}. The arrows pointing upwards identify the FeF_3 reflections. The pattern from the highest dose is shown enlarged in (b) with the FeF_3 and FeF_2 reflections identified.

the positions of the FeF_2 and FeF_3 rings. The electron diffraction patterns were quantified by digitizing and radially averaging to obtain the intensity as a function of the inverse of the d spacing [Fig. 2(a)]. The quantification of the radially averaged diffraction patterns is discussed in a previous paper.[7] The crystalline reflections appearing for doses below $\sim1.0\times10^6$ C m^{-2} correspond to FeF_2, while the extra reflections that appear at higher doses are from FeF_3, and are arrowed in Fig. 2(b).

Tables I and II show x-ray powder diffraction data for FeF_2 and FeF_3, respectively. All the FeF_2 and FeF_3 peaks which were identified in Figs. 1(d) and 2(b) are shown as bold and underlined in the Tables I and II, respectively. A few other peaks of FeF_2 and FeF_3 could not be identified accurately in the radially averaged diffraction patterns because they were closely spaced and hence could not be resolved. X-ray powder diffraction data from various oxides and hydroxides of iron were also compared to make sure of their absence in these diffraction patterns.

The appearance of FeF_2 first and FeF_3 (a fluorine-rich compound) later in the electron beam-induced crystallization process in the amorphous film is interesting. The appearance of FeF_2 before FeF_3 is probably due the nature of the crystal structure in these compounds. FeF_2 is a simple rutile structure (tetragonal, $a=4.7$ Å, $c=3.31$ Å) with a small unit cell, whereas FeF_3 has a complex ReO_3 type structure (hexagonal, $a=5.2$ Å, $c=13.32$ Å) with a large unit cell. Due to the small unit cell of FeF_2, short range diffusion and atomic rearrangement are required for its nucleation whereas much longer range diffusion is required for FeF_3. Hence, it is quicker to form FeF_2 under the beam than FeF_3.

In crystalline FeF_3 and FeF_2, the Fe^{3+} and Fe^{2+} ions sit in the center of FeF_6 octahedra, the difference being the octahedra in FeF_3 are linked *only* at the corners and in FeF_2, at the corners as well as edges. So, it is very easy to amorphise FeF_3 by just rotating each octahedron at the vertices by a

TABLE I. X-ray powder diffraction data for crystalline FeF_2. The bold and underlined reflections are the ones which are identified in Fig. 1(d).

d spacing Å	Intensity	h k l
3.32	**100**	**1 1 0**
2.70	**30**	**1 0 1**
2.344	**20**	**1 1 1**
		2 0 0
2.101	**6**	**2 1 0**
1.773	**40**	**2 1 1**
1.660	**4**	**2 2 0**
		0 0 2
1.488	8	3 1 0
		2 2 1
1.482	8	1 1 2
1.417	**10**	**3 0 1**
1.356	4	2 0 2
1.213	4	3 2 1
1.173	4	2 2 2
1.108	2	3 1 2
1.050	2	4 2 0
		3 3 1

TABLE II. X-ray powder diffraction data for crystalline FeF_3. The bold and underlined reflections are the ones which are identified in Fig. 1(d).

d spacing Å	Intensity	*h k l*
3.731	**100**	**0 1 2**
2.678	**15**	**1 0 4**
2.602	7	1 1 0
2.244	**14**	**1 1 3**
2.133	2	2 0 2
1.866	**21**	**0 2 4**
1.688	**21**	**1 1 6**
1.688	**21**	**2 1 1**
1.648	10	1 2 2
1.561	3	0 1 8
1.515	6	2 1 4
1.501	5	3 0 0
1.434	1	1 2 5
1.338	5	2 0 8
1.299	2	2 2 0
1.286	1	1 1 9
1.277	3	1 0 10
1.269	1	2 1 7
1.243	2	3 0 6
1.243	2	1 3 1

small amount with respect to the other. The thermally deposited FeF_2 film is microcrystalline at room temperature.

Figures 3(a) and 3(b) show electron energy loss spectra for crystalline and amorphous FeF_3 and crystalline and a thermally evaporated microcrystalline film of FeF_2, respectively. The crystal field splitting of 1.9 eV is seen in each of

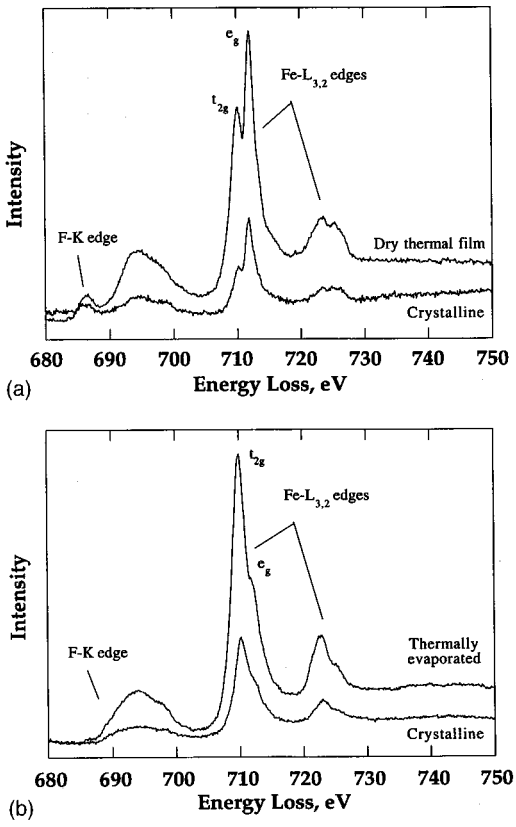

FIG. 3. EELS spectra of crystalline and thermally evaporated (a) FeF_3 and (b) FeF_2, respectively.

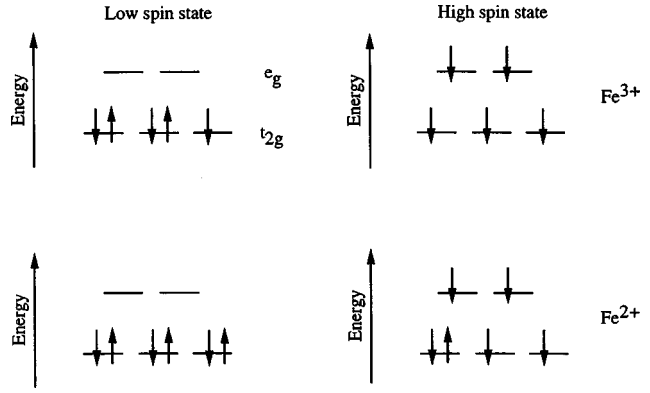

FIG. 4. Simple ligand field study of the Fe $L_{3,2}$ edges observed in Fig. 3.

the two peaks of Fe $L_{3,2}$ white lines of FeF_3 and FeF_2 suggesting that amorphous FeF_3 contains FeF_6 octahedra, like crystalline FeF_3, with the octahedra being randomly arranged in the amorphous material. Krishnan used a simple ligand field approach to study the EELS spectra of Fe^{3+} and Fe^{2+} in an octahedral coordination in oxides, assuming low spin state of the ions.[13] In the case of Fe^{3+} in an octahedral coordination, in addition to the empty e_g levels, there is an unpaired electron in the t_{2g} level. This was used to interpret the splitting of Fe $L_{3,2}$ edges in the case of Fe^{3+} in an octahedral environment (Fig. 4). For Fe^{2+} ions in an octahedral coordination, the six available electrons completely occupy the doubly degenerate e_g level. Hence, no peak splitting is observed in this case (Fig. 4). In the case of FeF_3 and FeF_2, where Fe^{3+} and Fe^{2+} are in octahedral coordination, the splitting of the Fe $L_{3,2}$ edges is clearly observed (Fig. 3). Assuming the low spin state of Fe^{3+} in FeF_3, the observed splitting of the L_3 edge can be explained, whereas the relative heights of the splitting peaks of the L_2 edge cannot be explained. But for the Fe^{2+} ion in FeF_2, neither the high spin nor the low spin state of iron ions explains the observed spectra satisfactorily (Fig. 4). In this case, the low spin state of the iron ion should not show any crystal field splitting, whereas a high spin state should show almost equal splitting of the Fe $L_{3,2}$ edges. This is not observed in the actual EELS spectrum [Fig. 3(b)]. Hence, in the present case, splitting cannot be explained by using a simple ligand field approach. A more detailed analysis would need to take into consideration the nature of the arrangement of octahedra in FeF_3 and FeF_2. In the former case, the octahedra are linked *only* at the corners and in the latter, at the corners as well as edges. The closeness of Fe^{2+} ions in FeF_2 can result in some interaction between iron ions. This will result in changes in the band structure of the material which could be calculated. This then could be used to model the spectra more accurately. Also, the energy resolution of EELS spectra was poor in Krishnan's work.[13] This is another possible reason why he did not see any crystal field splitting in the coreloss spectrum of Fe^{2+} ions in an octahedral coordination.

The EXAFS and XANES studies have shown that FeF_6 octahedra in FeF_3 are weakly distorted.[10] The calculated shapes of Fe $L_{3,2}$ peaks resulting from octahedrally coordinated Fe^{3+} and Fe^{2+} agree very well with our data.[14] The

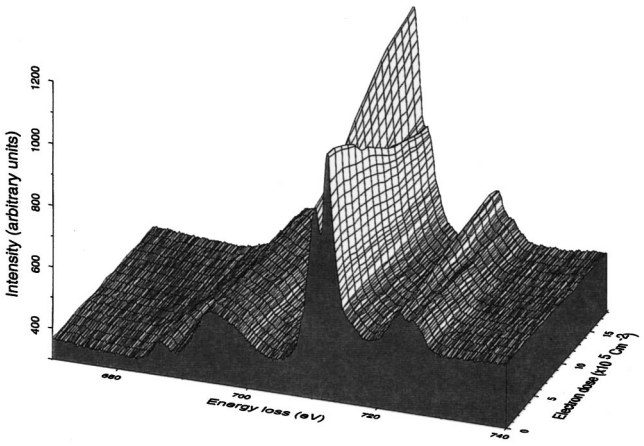

FIG. 5. Time-resolved EELS study of the amorphous to crystalline transition in FeF_3.

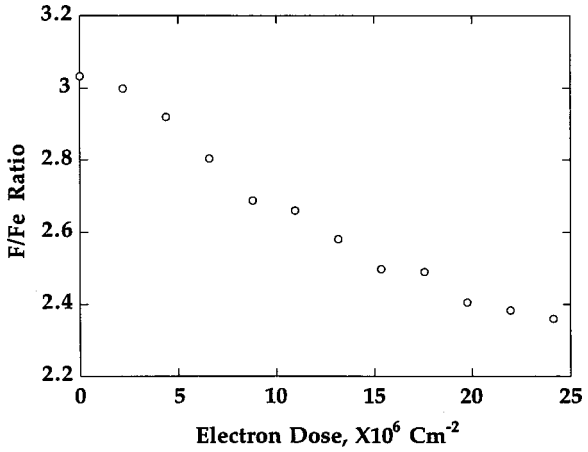

FIG. 6. Time-resolved F/Fe ratio with increasing electron dose calculated from Fig. 5.

fact that there is a pre-peak at the $F-K$ edge in FeF_3 due to the mixing of the F–$2p$ with Fe–$3d$ electrons indicates that there are significant covalent effects in this material. This peak is not present in FeF_2 and this is consistent with the fact that the Fe–$3d$ band is more empty in FeF_3 than in FeF_2, thus allowing the transitions to more empty $3d$ states to be visible.

Time-resolved electron energy loss spectroscopy of the amorphous to crystalline transition show that with increasing electron dose the lower energy white line intensity in L_3 and L_2 peaks increases whereas that of the higher energy white line decreases (Fig. 5). During this process, the crystal field splitting remains constant at 1.9 eV suggesting that the Fe ion remains octahedrally coordinated to fluorine during crystallization. The change in the intensity of the crystal field split peaks on the L_3 and L_2 edges and the decrease of the $F-K$ pre-edge is indicative of the change in the oxidation state as well as the composition of the film under the electron beam and is corroborated by the SADPs shown in Fig. 1. At higher doses, the Fe $L_{3,2}$ as well as fluorine K edges resemble thermally evaporated FeF_2 [Fig. 3(b)]. From the diffraction patterns from dry thermal film, it is clear that both FeF_2 and FeF_3 appear during crystallization (Fig. 1). Quantitative analysis of the time-resolved EELS spectra shows that the F/Fe ratio drops from 3 to about 2.4 (Fig. 6) pointing to a mixture of FeF_2 and FeF_3 in the crystallized area. On the other hand, the EELS spectra at higher doses suggests the presence of a large amount of FeF_2. The presence of a large amount of FeF_2 can effectively swamp the spectrum from FeF_3 which may be present in smaller amounts. A similar change in the intensity of crystal field split peaks was seen in the hole drilling studies of crystalline FeF_3 by a focused electron probe in a VG STEM.[8] Irradiation damage resulted in the deposition of iron on the walls of the hole which presumably changed the concentration as well as the oxidation state of iron ions in the vicinity of the hole.

Crystalline FeF_3 has the same crystal structure as that of AlF_3 but the damage behavior of the amorphous state of these fluorides under the electron beam is slightly different. Hole drilling studies of a-FeF_3 and AlF_3 using an intense nanoprobe in a VG STEM show ''popping type'' drilling, which exhibits an abrupt mass loss behavior. This tends to be associated with the displacement of dissociated ions from the irradiated volume and anion aggregation to form bubbles of fluorine gas.[8,15] The electron beam damage of a-AlF_3, using a broad electron probe, is a very complicated process, whereby crystalline Al is formed first as the fluorine is lost, followed by the crystallization of the a-AlF_3. At higher doses, the oxygen or presumably the moisture in the vacuum or in the specimen reacts with AlF_3 to form textured crystalline Al_2O_3. The water content as well as the deposition conditions greatly alter the doses required for each substance to crystallize.[6] Amorphous FeF_3 shows similar behavior with respect to water content and deposition conditions for the different dose requirement for crystallization under the electron beam. The presence of moisture in the film results in an increased dose requirement for crystallization.[7] It is seen that crystallization of thermally evaporated a-FeF_3 requires a higher electron dose than electron beam-deposited films.

In order to observe the changes in d-band occupancy during the amorphous to crystalline transition, the continuum part of the atomic cross section distribution due to fluorine was removed first (calculated with Egerton's SIGMAL programs available in the El/P 3.0 software[16]) and then a similar procedure was carried out on the Fe $L_{3,2}$ edges. The normalization to the continuum was carried out in the energy interval just after the L_2 white line so as to minimize the influence of multiple scattering which is of increased significance at higher energies relative to the threshold (Fig. 7). Intensities were measured by integrating the counts under the peaks after the continuum subtraction, the minimum in the troughs between the peaks being used to define the window widths. The normalized integrated intensity was then plotted against the electron dose as shown in Fig. 8. It is clear that with increasing electron dose, the d-band occupancy increases suggesting that on an average, the ionization states of Fe^{3+} changes to Fe^{2+}. This demonstrates that EELS is a powerful technique to observe changes in the d-band occupancy by amounts as small as one electron.

It has been shown that the ratio of the two spin-orbit components from the $2p_{3/2}$ and $2p_{1/2}$ transitions do not follow the statistical 2:1 ratio expected from the ratios of the

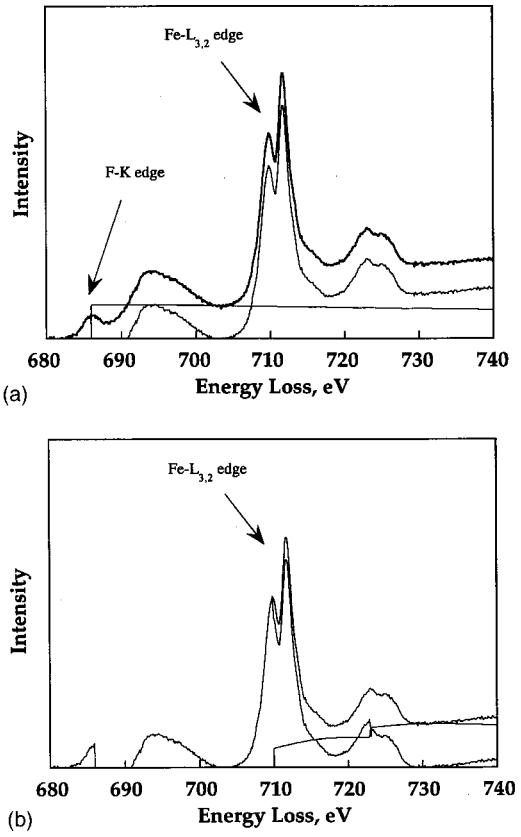

FIG. 7. Quantification of the Fe $L_{3,2}$ edge using the continuum subtraction. The background spectrum was used to subtract the continuum cross section calculated using the SIGMAL program to remove the contribution from the (a) fluorine *K* edge and (b) Fe $L_{3,2}$ edges.

initial state.[17,18] The ratio between the L_3 and L_2 lines can be quite sensitive to the electronic configuration and hence the charge state of the transition metal cation. This is especially true for the elements in the middle of the Periodic Table.[19] The variation of the ratio should be distinguishable even for a relatively small change in the electron concentration in the *d* band. Figure 9 shows the variation of the ratio between L_3 and L_2 lines versus the electron dose. This is also consistent with the change in average ionization state of iron ions from

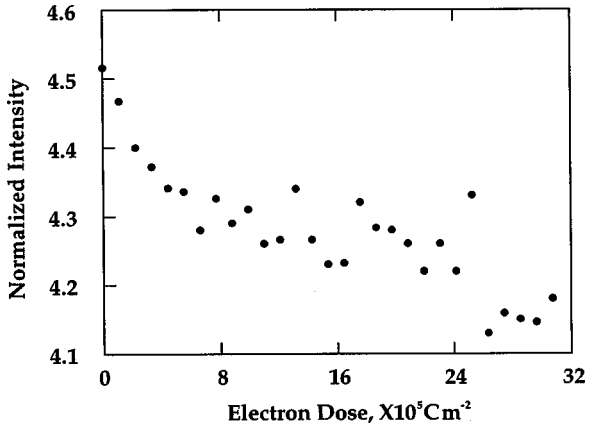

FIG. 8. Plot of normalized intensity versus the electron dose showing the sensitivity in the change of oxidation state with increasing electron dose.

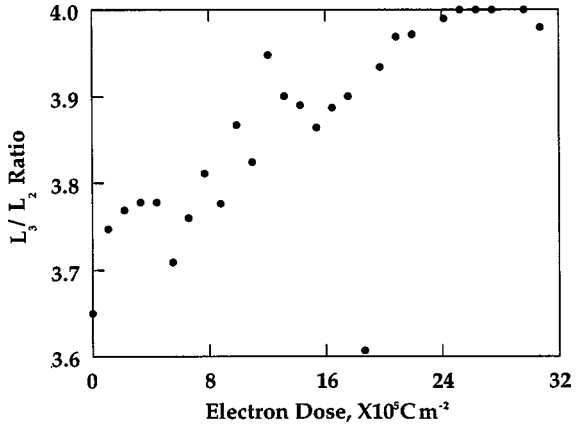

FIG. 9. Variation of the white line ratios with the electron dose.

Fe^{3+} to Fe^{2+}. It is seen that even a change of one electron is the *d* band is clearly manifested when the Fe^{3+} ions transform into Fe^{2+} ions during the amorphous to crystalline transition under the electron beam.

IV. CONCLUSIONS

It is shown using EELS that randomly arranged octahedral coordination is retained in amorphous FeF_3 and during crystallization under the beam these FeF_6 octahedra arrange themselves to form FeF_2 and FeF_3. The change in the *d*-band occupancy by one electron as well as the sensitivity of the ratio of Fe L_3 and L_2 edges to the charge state of the iron ion is clearly demonstrated using EELS. A simple explanation of the EELS spectra of FeF_3 and FeF_2 using a ligand field approach does not appear to be valid here.

ACKNOWLEDGMENTS

One of the authors (M.S.M.S.) would like to thank the Cambridge Nehru Trust for the financial support, Professor A. Moodie and Dr. A. R. Preston for stimulating discussions, and Dr. R. Harris for the help in drawing the plots.

[1] J. Fujita, H. Watanabe, Y. Ochiai, S. Manako, J. S. Tsai, and S. Matsui, Appl. Phys. Lett. **66**, 3064 (1995).
[2] H. Watanabe, J. Fujita, Y. Ochiai, S. Matsui, and M. Ichikawa, Jpn. J. Appl. Phys., Part 1 **34**, 6950 (1995).
[3] E. Kratschmer and M. Isaacson, J. Vac. Sci. Technol. B **5**, 369 (1987).
[4] W. Langheinrich, B. Spangenberg, and H. Beneking, J. Vac. Sci. Technol. B **10**, 2868 (1992).
[5] G. S. Chen, C. B. Boothroyd, and C. J. Humphreys, Inst. Phys. Conf. Ser. **138**, 369 (1993).
[6] G. S. Chen, C. B. Boothroyd, and C. J. Humphreys, Appl. Phys. Lett. **69**, 170 (1996).
[7] M. S. M. Saifullah, C. B. Boothroyd, G. A. Botton, and C. J. Humphreys, edited by J. S. Im, B. Park, A. L. Greer, and G. B. Stephenson, Mater. Res. Soc. Symp. Proc. **398**, 195 (1996).
[8] M. S. M. Saifullah, C. B. Boothroyd, C. J. Morgan, and C. J. Humphreys, Inst. Phys. Conf. Ser. **147**, 325 (1995).
[9] M. Eibschütz, M. E. Lines, L. G. Van Ultert, H. J. Guggenheim, and G. J. Zydzik, Phys. Rev. B **29**, 3843 (1984).
[10] J. M. Greneche, A. Le Bail, M. Leblanc, A. Mosset, F. Varret, J. Galy, and G. Ferey, J. Phys. C **21**, 1351 (1988).
[11] D. H. Pearson, B. Fultz, and C. C. Ahn, Appl. Phys. Lett. **53**, 1405 (1988).
[12] J. Taftø and O. L. Krivanek, Phys. Rev. Lett. **48**, 560 (1982).
[13] K. M. Krishnan, Ultramicroscopy **32**, 309 (1990).

[14] G. van der Laan and I. W. Kirkman, J. Phys.: Condens. Matter **4**, 4189 (1992).
[15] G. S. Chen, Ph.D thesis, University of Cambridge (1995).
[16] R. F. Egerton, *EELS in the Electron Microscope* (Plenum, New York, 1996).
[17] R. D. Leapman and L. A. Grunes, Phys. Rev. Lett. **45**, 397 (1980).
[18] R. D. Leapman, L. A. Grunes, and P. L. Fejes, Phys. Rev. B **26**, 614 (1982).
[19] W. G. Waddington, P. Rez, I. P. Grant, and C. J. Humphreys, Phys. Rev. B **34**, 1467 (1986).